Dielectrophoresis-actuated liquid lenses with dual air/liquid interfaces tuned from biconcave to biconvex

Qingming Chen[ab], Tenghao Li[a], Zhaohui Li[c], Chao Lu[*b] and Xuming Zhang[*a]

*Corresponding Author: E-mail: enluchao@polyu.edu.hk; apzhang@polyu.edu.hk

[a]Department of Applied Physics, The Hong Kong Polytechnic University, Hong Kong, China
[b]Department of Electronic and Information Engineering, The Hong Kong Polytechnic University, Hong Kong, China
[c]School of Electronics and Information Technology, Sun Yat-Sen University, Guangzhou 510275, China

Abstract: This paper reports an electrically reconfigurable optofluidic lens with two air-liquid (silicone oil) interfaces actuated by the dielectrophoretic (DEP) force. Initially, a symmetric biconcave air-liquid lens is formed by the surface tension in a microfluidic chip. Then, the DEP force deforms the air-liquid interfaces from biconcave to biconvex, tuning the focal length from -0.5 mm to infinite to +0.5 mm. The wide tunability of the focal length is resulted from the large refractive index difference (~0.4 at air-liquid interface), which is only 0.1 in the previous liquid-liquid lenses. In the experiment, it achieves an *f* number of 0.91 while consumes only 6.7 nJ/circle. Some asymmetric working states, such as concave-convex and plano-convex lenses have also been demonstrated. Compared with the continuous liquid flow sustained lenses, this stationary liquid lens promises better compatibility and higher scalability. The wide tunability, low power consumption and easy operation make it suitable for light manipulation in microfluidic networks.

1. Introduction

Optofluidics combines optics and microfluids together to make use of the interaction between light and liquid samples in microscale.[1-7] Due to its compact size and flexible tunability, optofluidics has unprecedented advantages over the conventional counterparts, such as small volume sample handling,[8-13] precise manipulation,[14-18] wide tunability[19-21] and lab-on-a-chip integration.[22-25] As the key element in conventional optics, optical lens has attracted intense attention in optofluidics.[26-28] Several types of adaptive liquid lenses have been successfully developed for different applications, such as miniature camera,[29-31] particle manipulation[32] and flow cytometers,[33-34-] etc. Among them, the in-plane liquid lens that deals with the beams propagating along the substrate, has been widely used in the light manipulation in microfluidic networks.[35-37]

The previous in-plane liquid lenses are based on refractive index (RI) gradient using solution diffusion[37-39] or interfaces between immiscible liquid flows[26,40]. The fluidic interfaces can be manipulated by several types of microfluidic methods, such as hydrodynamic flow,[40] pressure control[41] and electrostatic force,[42] etc. Among them, the hydrodynamic flow has been widely used to control the in-plane optofluidic lenses. The optical smoothness of the fluidic interface makes it suitable for light manipulation without significant scattering loss. Generally, the lens is formed by the immiscible flowing streams with different RIs, where the liquid with higher RI as the core and the one with lower RI as the cladding. The lens shape (or focal length) can be continuously tuned by changing the flow rate, providing a flexible way to manipulate light in microfluidic networks. By injecting flow streams into chambers with rectangle or circular shapes, several reconfigurable lenses have been demonstrated.[43-46] Seow *et al.* proposed a reconfigurable liquid lens by tuning flow rates of three laminar streams in a rectangle expansion chamber, which obtained different curvatures of liquid/liquid interfaces.[44] To get a perfect curvature, a circular chamber was used in a liquid-core/liquid-cladding lens. The shape can be tuned from the radius of the chamber itself to infinite via the flow rate control.[45] Fang et al. reported a reconfigurable optofluidic lens, which was hydrodynamically tuned from biconvex to biconcave.[46] It utilized a rectangle chamber with two semicircular terminals that connected to two inlets and two outlets. By adjusting the flow rates of four streams, the beam was continuously tuned from focusing to collimation and then to divergence. The above designs have demonstrated flexible manipulation of light in microfluidic chips. But there are still some constraints in the previous optofluidic systems. For instance, they are sustained by continuous liquid supply or flow circulation,[47] which reduces the scalability of the lenses. In addition, the focal length tunability is limited by the small RI difference (~0.1) between liquids.[35] Thus, more practical designs of in-plane optofluidic lens are still in need.

This paper presents a tunable in-plane liquid lens using the DEP force, which drives the liquid (silicone oil, ε = 2.5, n = 1.405) with higher permittivity into the air region with lower permittivity.[48-49] It can be continuously tuned from biconcave to biconvex. The large RI difference (~0.4) at the air-liquid interface leads to a wider tunable range of the focal length from -0.5 mm to infinite and then to +0.5 mm. Some asymmetric working states, such as plano-convex and concave-convex lenses can also be achieved. In addition, it does not require continuous liquid flow, making it highly scalable in the microfluidic networks.

2. Working principle

The schematic design of the liquid lens is shown in Fig. 1. Two parallel MgF_2 glasses are bonded together to form the microfluidic platform, where the NOA 81 (Norland Optical Adhesive 81) works as the spacers and defines two open channels (along x direction). At the center of the chip, there is a lens section ($w_0 \times l_0 \times d_0$ = 550×1000×60 μm^3) between the four spacers. The top glass is patterned with ITO electrodes, including an ITO line (in x direction) between the two channels and a pair of ITO patterns (in y direction). The ITO line is used to apply a DEP force (voltage: V_0) to guide the liquid droplets from the two inlets to merge at the lens section, resulting in a biconcave air-liquid lens (as shown in the inset of Fig. 1). And the ITO pair (V_1 & V_2) are used to exert DEP forces at the air-liquid interfaces to deform the lens shape (see the blue liquid). V_1 and V_2 pull the air-liquid interfaces in the -y and +y directions, respectively. The lens shape can be continuously tuned from biconcave to biconvex by the DEP force. To observe the lensing effect, A collimated beam (λ = 532 nm, waist diameter = 400 μm) is coupled into the chip using a pigtailed aspheric fiber collimator (CFS2-532-FC, beam divergence 1.75 mrad, Thorlabs). And a chamber (not included in the schematic) is fabricated behind the lens section for experimental raytracing. The details of the device fabrication can be found in the supplementary information.

Initially, the shape of the liquid droplet is determined by the surface tension. The pressure drop at the air-liquid interface can be described by the Laplace law [50]:

$$\Delta P_0 = 2\gamma\kappa = \gamma\left(\frac{1}{R_{10}} + \frac{1}{R_{20}}\right) \quad (1)$$

where ΔP_0 is the pressure drop, γ is the surface tension between air and the liquid ($\gamma_{\text{silicone oil}}$ = 20 mN·m^{-1}), and κ is the mean curvature. R_{10} and R_{20} are the curvature radii in the horizontal and vertical directions, respectively. As the device is symmetric along the x & y axes, the two air-liquid interfaces have the same physical properties. When a voltage is applied to the ITO pair, it exerts a net force at the air-liquid interfaces to deform the shape of the droplet. The DEP force at one air-liquid interface is:

$$F_e = \frac{\varepsilon_0\left(\varepsilon_L - 1\right)w_1}{2d_0}V^2 \quad (2)$$

where $\varepsilon_0 = 8.8542\times10^{-12}$ F·m^{-1} is the permittivity of vacuum and ε_L ($\varepsilon_{\text{silicone oil}}$ = 2.5) is the relative permittivity of the liquid, w_1 is the width of the top electrode and d_0 is the height of the channel. V represents the applied voltage. The external force breaks the balance state of the interface, resulting in a different pressure drop and curvature:

$$\Delta P_1 - \Delta P_0 = \gamma\left(\frac{1}{R_{11}} + \frac{1}{R_{20}}\right) - \gamma\left(\frac{1}{R_{10}} + \frac{1}{R_{20}}\right) = \gamma\left(\frac{1}{R_{11}} - \frac{1}{R_{10}}\right) \quad (3)$$

here R_{10} and R_{11} are the horizontal curvature radii of the initial and new states, respectively.

And ΔP_1 is the pressure drop of the new static state. As the surface tension of the top and bottom glasses keep unchanged, the vertical curvature radius R_{20} is constant at the static states. And the DEP force is balanced by the surface tension:

$$F = \left(\Delta P_1 - \Delta P_0\right) w_0 d_0 = F_e \tag{4}$$

where w_0 is the distance between the terminals of the two channels. Thus $S = w_0 d_0$ is the y-direction projection of an air-liquid interface. The horizontal radii of the new interfaces are determined by Equations (1) – (4). If $V_1 = V_2$, the liquid lens is at symmetric state, which means that the two air-air interfaces have the same curvature radius in magnitude. Since the width of the lens is not negligible in comparison with the curvature radius, it cannot be regarded as a thin lens. The optical properties of the liquid lens follow the Snell law. Thus, the lens can be considered as two separated air-liquid interfaces, where the rays bend according to the Snell law. The rays propagate along the straight lines inside and outside of the lens. Fig. 2 displays the optical model of the biconcave and biconvex liquid lenses in this paper.

In Fig. 2a, the parallel rays diverge after passing the biconcave lens, which seem to be from a back focal point F'_0. While in the biconvex lens, the parallel rays are focused into a point F_0, see Fig. 2b. The two red lines (H_1 & H_2) in Fig. 2 indicate the two principal planes of the lens. And the effective focal length f can be expressed as

$$\frac{1}{f} = \left(n-1\right)\left[\frac{1}{R_1} - \frac{1}{R_2} + \frac{\left(n-1\right)d}{nR_1R_2}\right] \tag{5}$$

where n is the RI of the liquid, R_1 and R_2 are the radii of the first and second interfaces, respectively. And d is the thickness of the lens. The positions of the two principal planes are determined by:

$$h_1 = -\frac{f\left(n-1\right)d}{nR_2} \tag{7}$$

$$h_2 = -\frac{f(n-1)d}{nR_1} \quad (8)$$

3. Simulated and experimental results

The lens has been verified by both theoretical calculations and experimental results. At first, some theoretical calculations have been conducted to optimize the design of the liquid lens. Then it is demonstrated by the experiments.

3.1. Measurement of air-liquid interfaces

At first, some experiments have been conducted to measure the air-liquid interfaces under different voltages. Initially, a biconcave lens is formed in the microfluidic chip, as shown in Fig. 3a. The two air-liquid interfaces have the same curvature radius (0 V, |R| = 485 μm) due to the symmetric design. Then a voltage is applied to modify the curvature of the liquid lens. At first, the magnitude of the radius increases with an increasing voltage, see Fig. 3b (100 V, |R| = 718 μm). When the voltage is at 175 V, a planar lens appears (Fig. 3c). Further increase the voltage turns it into a biconvex shape, as shown in Fig. 3d (240 V, |R| = 556 μm). In the focusing states, the magnitude of the radius reduces as increasing the voltage. For comparison, the calculated spherical curves (red dashed curves) are put together with the corresponding experimental results in Fig. 3a-d. It is noticed that the experimental interfaces closely match the theoretical curves. For easy visualization, the raytracing simulation of the liquid lens at 240 V is shown in Fig. 3e, which demonstrates the focusing effect of the liquid lens.

3.2 Experimental raytracing

In order to clearly trace the beam, a chamber is fabricated behind the lens. It is filled with the mixer of NOA 81 and Rhodamine B for fluorescent imaging. At first, the liquid lens has a biconcave shape resulted from the surface tension. As shown in Fig. 4a, the beam becomes divergent after passing the biconcave lens. When the voltage gradually increases from 0 V, the lens is deformed by the DEP force. At 175 V, it becomes a planar lens, which does not have focusing effect. As shown in Fig. 4b, the parallel beam keeps unchanged. Further increase the voltage, the lens turns into a biconvex one. Thus, the focusing appears as shown in Fig. 4c (210 V, f = 1.6 mm). The focal length of about 0.5 mm is obtained at 250 V (see Fig. 4d). The raytracing results demonstrate great focusing performance of the DEP lens.

3.3. Tunability of liquid lens

The tunability of the DEP lens is verified by the calculations as well. The curvature of the liquid-air interfaces is deduced by the Laplace law and the DEP force at the interfaces. Then the thick lens model is used to calculate the focal length. Fig. 5 plots both the calculated and experimental results. The curves are the theoretical prediction and the data points (each represents the average of five measurements) are the experimental results. At first, the focal length decreases from -0.5 mm to infinite while the voltage is increased from 0 V to 175 V, see the blue curve in Fig. 5. With further increase of the voltage, the focal length is gradually reduced from infinite to +0.5 mm (250 V). For easy visualization, the micrographs of four working states are inserted into Fig. 5.

3.4 Asymmetric working states

This DEP lens can not only work at symmetric states, but also at asymmetric states that the two air-liquid interfaces have different curvatures.The asymmetric tuning enables independent manipulation of lens' interfaces, providing a new freedom of tunability. Fig. 6a shows the planar lens when both voltages are 175 V, which has no lens effect. While one interface is under 0 V and the other is at 175 V, a concave-convex is obtained. As the concave and convex curves share the same magnitude of radius (i.e., |R| = 626 μm), the probe beam keeps collimated after passing the lens, see Fig. 6b. A plano-convex lens is achieved by applying 225 V and 262 V at the left and right (R = 416 μm) interfaces, respectively. It has a focal length of about 1.2 mm, see Fig. 6c.

3.5 Power consumption, repeatability, *f* number and response time

The silicone oil is chosen as the optical medium because of its unique properties, such as high transparence,[51] low evaporation rate, low viscosity and high electrical insulation. The optically smooth interface and the low absorption lead to a low optical loss. And the low evaporation rate of the liquid makes the lens well repeatable for one month. Since the silicone oil layer has a very high electrical resistance (over 500 MΩ), the device can be regarded as a capacitor (0.55 mm × 1.05 mm × 0.06 mm). The energy consumption is as low as 6.7 nJ per switching circle. The proposed liquid lens also has a large *f* number, which is define as *f* / D (the aperture is 0.55 mm). At 250 V, the smallest focal length is about 0.5 mm, resulting in an *f* number of 0.91. But the response speed of the lens is slow due to the edge pinning effect, which is related with the size of the device and the viscosity of the liquid. It takes about 6 s to switch from -0.5 mm to +0.5 mm. While the response speed can be improved by reducing the size of the lens or choosing a liquid with lower viscosity.

4 Conclusion

In conclusion, a new DEP-actuated in-plane lens has been presented. It demonstrates the continuous modulation of focal length from -0.5 mm to infinite and then to +0.5 mm when the lens is changed from biconcave to planar and then to biconvex state. By using the asymmetric driving, concave-convex and plano-convex lenses have also been achieved. It is superior to the previous in-plane liquid lenses in various aspects, such as electrical actuation, stationary liquid and wide tunability. In addition, it obtains an *f*-number of 0.91 and consumes only 6.7 nJ per switching circle. Its flexible tunability and high scalability result in better compatibility with other microfluidic elements. This new design will find potential applications in lab-on-a-chip systems.

Conflicts of interest

There are no conflicts to declare.

Acknowledgements

This work is supported by National Natural Science Foundation of China (61377068), Research Grants Council of Hong Kong (N_PolyU505/13, 152184/15E, 152127/17E and 152126/18E), and Hong Kong Polytechnic University (G-YBPR, 4-BCAL, 1-ZE14, 1-ZE27 and 1-ZVGH).

References

[1] D. Psaltis, S. R. Quake and C. Yang, *Nature*, 2006, **442**, 381.

[2] X. Fan and I. M. White, *Nat. Photonics*, 2011, **5**, 591–597.

[3] C. Monat, P. Domachuk and B. J. Eggleton, *Nat. Photonics*, 2007 **1**, 106–114.

[4] D. Erickson, D. Sinton and D. Psaltis, *Nat. Photonics*, 2011, **5**, 583.

[5] X. Fan and S. H. Yun, *Nat. Methods*, 2014, **11**, 141.

[6] Y. Zhao, Z. S. Stratton, F. Guo, M. I. Lapsley, C. Y. Chan, S. C. S. Lin and T. J. Huang, *Lab Chip*, 2013, **13**, 17-24.

[7] C. Song and S. H. Tan, *Micromachines*, 2017, **8**, 152.

[8] H. Zhu, I. M. White, J. D. Suter, P. S. Dale and X. Fan, *Opt. Express*, 2007, **15**, 9139-9146.

[9] L. K. Chin, A. Q. Liu, Y. C. Soh, C. S. Lim and C. L. Lin, *Lab Chip*, 2010, **10**, 1072–1078.

[10] N. Wang, X. M. Zhang, Y. Wang, Y. Wang and H. L. W. Chan, *Lab Chip*, 2014, **14**, 1074-1082.

[11] N. Wang, X. M. Zhang, B. Chen, W. Song, N. Y. Chan and H. L. W. Chan, *Lab Chip*, 2012, **12**, 3983–3990.

[12] Y. Shi, H. Liu, X. Zhu, J. Zhu, Y. Zuo, Y. Yang, F. Jiang, C. Sun, W. Zhao and X. Han, *Lab Chip*, 2018, **18**, 2994-3002

[13] L. Liang, Y. Jin, X. Zhu, F. Zhou and Y. Yang, *Lab Chip*, 2018, **18**, 1422-1429

[14] Y. Shi, S. Xiong, Y. Zhang, L. Chin, Y. Chen, J. Zhang, T. Zhang, W. Ser, A. Larson, L. Hoi, J. Wu, T. Chen, Z. Yang, Y. Hao, B. Liedberg, P. Yap, D. Tsai, C. Qiu and A. Q. Liu, *Nat. Commun*, 2018, **9**, 815

[15] Y. Shi, S. Xiong, L. K. Chin, J. Zhang, W. Ser, J. Wu, T. Chen, Z. Yang, Y. Hao, B. Liedberg, P. H. Yap, D. P. Tsai, C. W. Qiu and A. Q. Liu. *Sci Adv*, 2018, **4**, eaao0773.

[16] K. Zhang, A. Jian, X. M. Zhang, Y. Wang, Z. Li and H.-Y. Tam, *Lab Chip*, 2011, **11**, 1389–1395.

[17] B. S. Schmidt, A. H. Yang, D. Erickson and M. Lipson, *Opt. Express*, 2007, **15**, 14322–14334.

[18] Y. Z. Shi, S. Xiong, L. K. Chin, Y. Yang, J. B. Zhang, W. Ser, J. H. Wu, T. N. Chen, Z. C. Yang, Y. L. Hao, B. Liedberg, P. H. Yap, Y. Zhang and A. Q. Liu, *Lab Chip*, 2017, **17**, 2443–2450.

[19] Y. Yang, A. Q. Liu, L. K. Chin, X. M. Zhang, D. P. Tsai, C. L. Lin, C. Lu, G. P. Wang and N. I. Zheludev, *Nat. Commun*, 2012, **3**, 651.

[20] Y. Yang, L. K. Chin, J. M. Tsai, D. P. Tsai, N. I. Zheludev and A. Q. Liu, *Lab Chip*, 2012, **12**, 3785–3790.

[21] S. K. Tang, B. T. Mayers, D. V. Vezenov and G. M. Whitesides, *Appl. Phys. Lett*, 2006, **88**, 061112.

[22] Y. Tung, M. Zhang, C. Lin, K. Kurabayashi and S. J. Skerlos, *Sens. Actuators B*, 2004, **98**, 356–367.

[23] H. Ren and S.-T. Wu, *Opt. Express*, 2008, **16**, 2646–2652.

[24] W. Song and D. Psaltis, *Lab Chip*, 2011, **11**, 2397–2402.

[25] P. Fei, Z. Chen, Y. Men, A. Li, Y. Shen and Y. Huang, *Lab Chip*, 2012, **12**, 3700-3706.

[26] N. T. Nguyen, *Biomicrofluidics*, 2010, **4**, 031501.

[27] C.P. Chiu, T.J. Chiang, J.K. Chen, F.C. Chang, F. H. Ko, C.W. Chu, S. W. Kuo and S. K. Fan, *J. Adhes. Sci. Technol*, 2012, **26**, 1773–1788.

[28] S. Xu, H.W. Ren and S.T. Wu, *J. Phys. D: Appl. Phys*, 2013, **46** , 483001.

[29] L. Liang, X. Zhu, H. Liu, Y. Shi and Y. Yang, *Lab Chip*, 2017, **17**, 3258-3263

[30] S. Kuiper and B. H. W. Hendriks, *Appl. Phys. Lett*, 2004, **85**, 1128-1130.

[31] B. H. W. Hendriks, S. Kuiper, M. V. As, C. A. Renders and T. W. Tukker, *Opt. Rev*, 2005, **12**, 255-259.

[32] H. L. Liu, Y. Shi, L. Liang, L. Li, S. S. Guo, L. Yin and Y. Yang, *Lab Chip*, 2017, **17**, 1280–1286.

[33] C. Song, T. D. Luong, T. F. Kong, N. T. Nguyen and A. K. Asundi, *Opt Lett*, 2011, **36**, 657-659.

[34] Y. Zhang, B. R. Watts, T. Guo, Z. Zhang, C. Xu and Q. Fang, *Micromachines*, 2016, **7**, 70.

[35] Q. Chen, T. Li, Z. Li, J. Long and X. M. Zhang, *Micromachines,* 2018, **9**, 97.

[36] X. Zhu, L. Liang, Y. Zuo, X. M. Zhang and Y. Yang, *Laser Photonics Rev*, 2017, **11**, 1770062.

[37] Y. Zuo, X. Zhu, Y. Shi, L. Liang and Y. Yang, *Micromachines*, 2018, **9**, 163.

[38] X. Mao, S.-C. S. Lin, M. I. Lapsley, J. Shi, B. K. Juluri and T. J. Huang, *Lab Chip*, 2009, **9**, 2050–2058.

[39] Q. Chen, A. Jian, Z. Li and X. M. Zhang, *Lab Chip*, 2016, **16**, 104-111.

[40] X. L. Mao, J. R. Waldeisen, B. K. Juluri and T. J. Huang, *Lab Chip*, 2007, **7**, 1303–1308.

[41] J. Shi, Z. Stratton, S. C. S. Lin, H. Huang and T. J. Huang, *Microfluidics & Nanofluidics*, 2010, **9**, 313-318.

[42] H. Li, C. Song, T. D. Luong, N. T. Nguyen and T. N. Wong, *Lab Chip*, 2012, **12**, 3680-3687.

[43] S. K. Tang, C. A. Stan and G. M. Whitesides, *Lab Chip*, 2008, **8**, 395-401.

[44] Y. C. Seow, A. Q. Liu, L. K. Chin, X. C. Li, H. J. Huang, T. H. Cheng and X. Q. Zhou, *Appl. Phys. Lett*, 2008, **93**, 084101.

[45] C. Song, N. T. Nguyen, S. H. Tan and A. K. Asundi, *Lab Chip*, 2009, **9**, 1178-1184.

[46] C. Fang, B. Dai, Q. Xu, R. Zhuo, Q. Wang, X. Wang and D. Zhang, *Opt. Express*, 2017, **25**, 888-897.

[47] E. E. Jung and D. Erickson, *Lab Chip*, 2012, **12**, 2575-2579

[48] S. K. Fan, H. P. Lee, C. C. Chien, Y. W. Lu, Y. Chiu and F. Y. Lin, *Lab Chip*, 2016, **16**, 847-854.

[49] Q. Chen, T. Li, Y. Zhu, W. Yu and X. M. Zhang, *Opt. Express*, 2018, **26**, 6532-6541.

[50] L. Hu, M. Wu, W. Chen, H. Xie and X. Fu, *Exp. Therm Fluid Sci*, 2017, **87**, 50-59.

[51] M. Xu, X. Wang, B. Jin and H. Ren, *Micromachines* 2014, *6*, 186-195

Figures

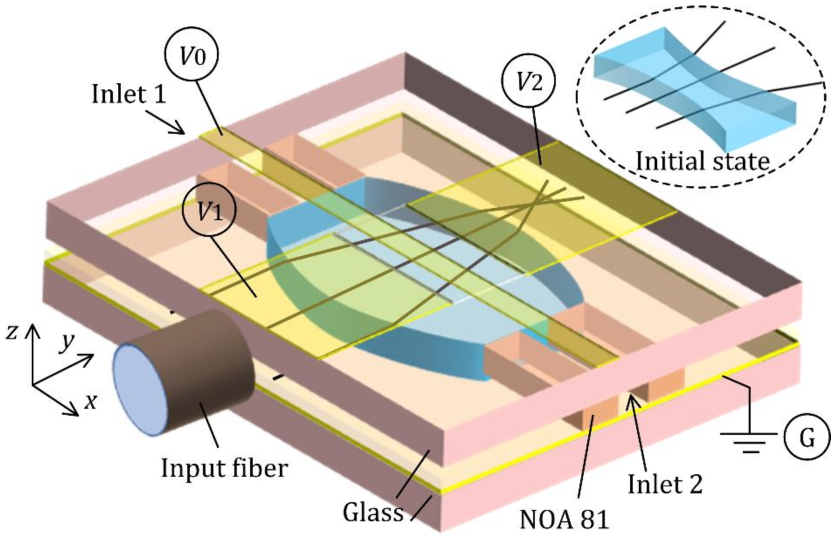

Fig. 1. Schematic design of the DEP lens. Two parallel glasses are bonded firmly by NOA 81 adhesive strips, forming two open microchannels. There is a disconnect part in the middle section, where the fluidic lens (the blue liquid) locates. V_0 is used to guide the capillary flows from the two inlets to merge at the center, forming a biconcave liquid lens (see the inset). Then, V_1 and V_2 deform the two liquid-air interfaces. A collimated beam is coupled into the chip by an input fiber.

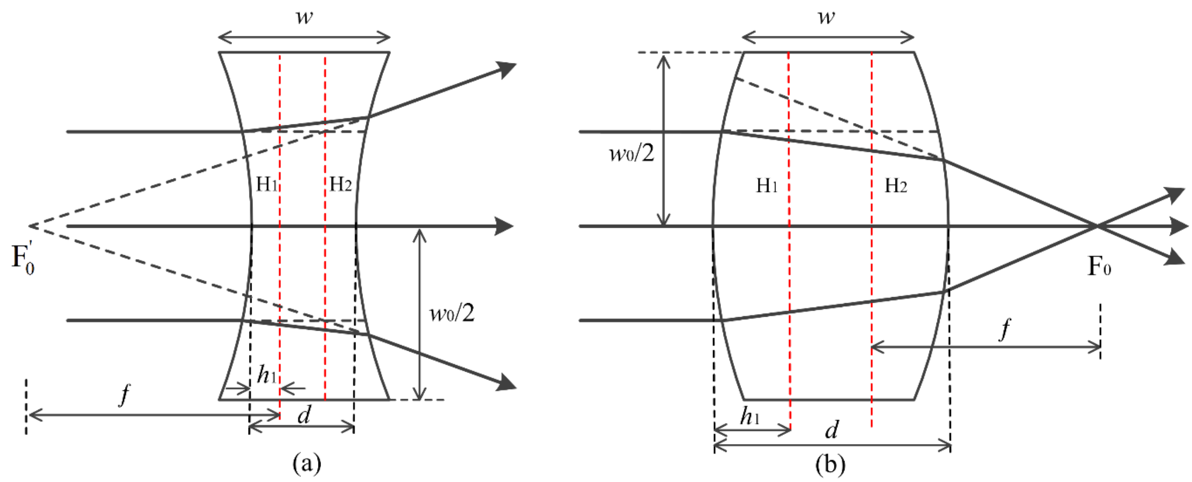

Fig. 2. Optical model of the DEP lens. w and w_0 are the width and length of the open section, respectively. H_1 and H_2 are the first and second principal planes. The distance between the two liquid-air interfaces is d. (a) Defocusing of the biconcave liquid lens. (b) Focusing of the biconvex lens.

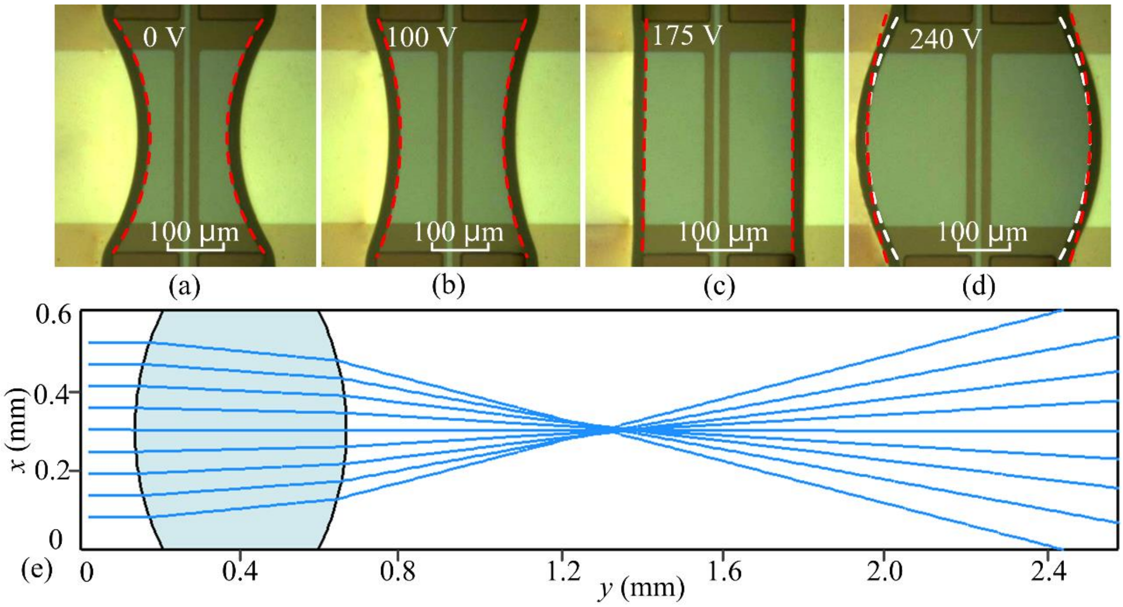

Fig. 3. Measured air-liquid interfaces under different applied voltages: (a) 0 V; (b) 100 V; (c) 175 V and (d) 240 V. The red dashed circle lines are the calculated results. And the white dashed lines in (d) represent the experimental curves. (e) Raytracing of the liquid lens of (d).

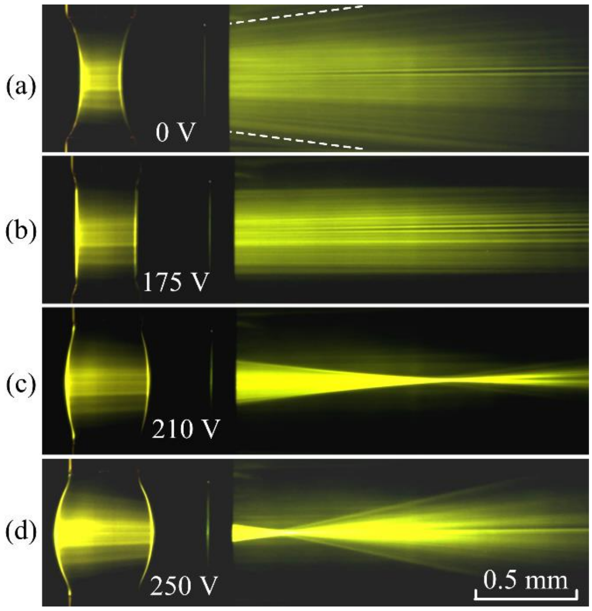

Fig. 4. Symmetric tuning. (a) Divergent state of the biconcave lens at 0 V. (b) Planar state at 175 V. (c) Focusing state of the biconvex lens at 210 V. (d) Tight focusing state at 250 V. (see ESI1)

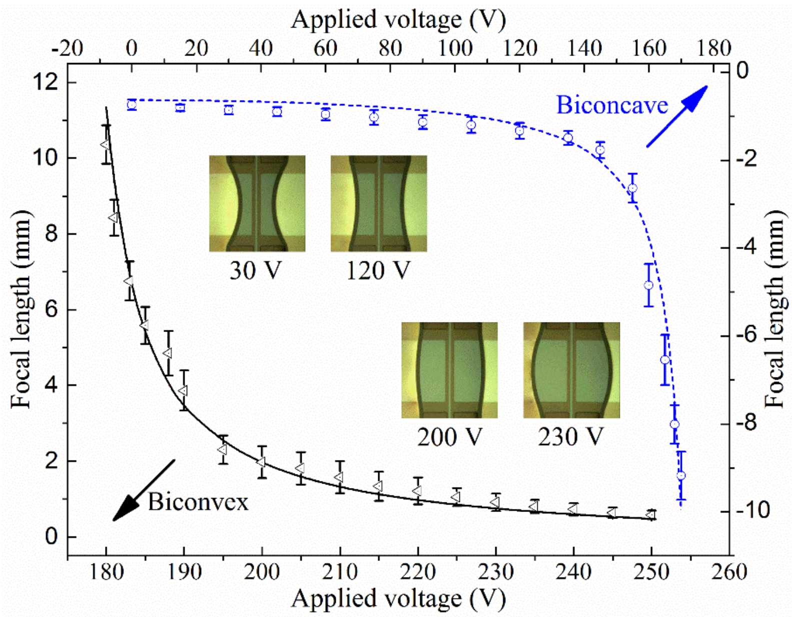

Fig. 5. The tunability of the focal length f. At first, when the voltage increases from 0 to 175 V, the focal length decreases from about -0.5 mm to infinite, see the blue line and the data points. Further increase the voltage, it tuns into a convergent lens. And focal length can be tuned from infinite to around +0.5 mm, see the black line and the data points. Here the lines are the theoretical predictions and the data points are the experimental results. Some lenses are inserted for easy visualization.

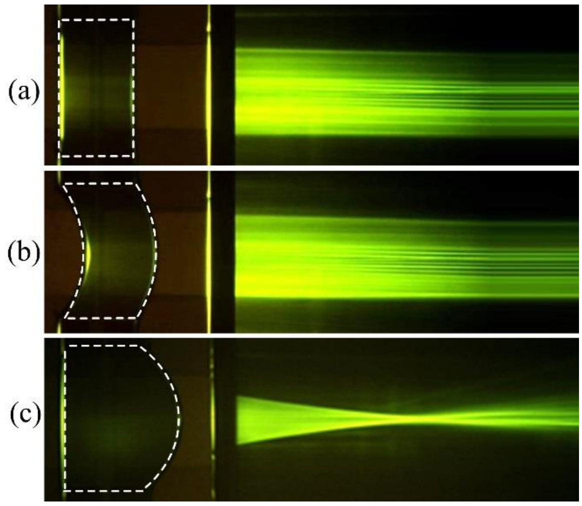

Fig. 6. Asymmetric tuning. (a) Planar lens at 175 V. (b) Concave-convex lens at 0 V-175 V and (c) Plano-convex lens at 225 V – 262 V. (see ESI2)